J. Cent. South Univ. (2021) 28: 2670−2686
DOI: https://doi.org/10.1007/s11771-021-4801-z

Springer

Effect of isothermal compression and subsequent heat treatment on grain structures evolution of Al-Mg-Si alloy

LI Ze-cheng(李泽程)[1, 2], DENG Yun-lai(邓运来)[2, 3], YUAN Man-fa(袁满发)[1, 2],
ZHANG Jin(张劲)[1, 2], GUO Xiao-bin(郭晓斌)[3]*

1. Light Alloy Research Institute, Central South University, Changsha 410083, China;
2. State Key Laboratory of High Performance Complex Manufacturing, Central South University, Changsha 410083, China;
3. School of Materials Science and Engineering, Central South University, Changsha 410083, China

Abstract: The constitutive relationships of Al-Mg-Si alloy deformed at various strain rates, temperatures and strains were studied. The microstructure evolution was quantitatively characterized and analyzed, including recrystallization fraction, grain sizes, local misorientation, geometrically necessary dislocation and stored strain energy during hot deformation and subsequent heat treatment. The results show that the dislocation density and energy storage are linear with ln$Z$ during hot deformation and subsequent heat treatment, indicating continuous recrystallization occurring in both processes. With higher ln$Z$, the dislocation density declines more sharply during subsequent heat treatment. When ln$Z$ is less than 28, dislocation density becomes more stable with less reduction during subsequent heat treatment after hot deformation. As these dislocations distribute along low angle grain boundaries, the subgrain has good stability during subsequent heat treatment. The main recrystallization mechanism during hot deformation is continuous dynamic recrystallization, accompanied by geometric dynamic recrystallization at higher ln$Z$.

Key words: Al-Mg-Si alloy; Zener-Hollomon parameter; dislocation; recrystallization; grain boundaries

Cite this article as: LI Ze-cheng, DENG Yun-lai, YUAN Man-fa, ZHANG Jin, GUO Xiao-bin. Effect of isothermal compression and subsequent heat treatmenton grain structures evolution of Al-Mg-Si alloy [J]. Journal of Central South University, 2021, 28(9): 2670−2686. DOI: https://doi.org/10.1007/s11771-021-4801-z.

1 Introduction

Aluminum alloys, especially the Al-Mg-Si series, are well recognized for their superior properties, such as high specific strength, proper corrosion resistance, adequate formability and low cost [1]. Compared with castings, aluminum alloy forgings have higher toughness and fatigue resistance due to their fibrous grain structure [2]. Therefore, they are widely used in aerospace, automotive and train structural components to reduce weight and thus fuel consumption.

In the processing of Al-Mg-Si aluminum alloy, solution and/or aging heat treatment is usually needed to induce precipitation-strengthening after hot deformation [3]. However, in the subsequent heat treatment process, the deformed microstructure

Foundation item: Project(2016YFB0300901) supported by the National Key R&D Program of China; Project(TC190H3ZV/2) supported by the National Building Project of Application Demonstration Platform on New Materials Products, China; Project (15308469779) supported by Key Laboratory of National Science and Technology for Equipment Pre-research, China
Received date: 2021-01-16; **Accepted date:** 2021-03-22
Corresponding author: GUO Xiao-bin, PhD, Associate Professor; Tel: +86-15111390850; E-mail: xiaobinguo@csu.edu.cn; ORCID: https://orcid.org/0000-0003-1708-838X

will further evolve and even lead to the formation of coarse grains. During the high temperature deformation of these alloys, the microstructure evolution is a dynamic process. The interaction between work hardening and thermal softening evolves with the deformation conditions, i.e. strain rate, temperature and strain, resulting in the change of dislocation density and microstructure [4, 5]. However, in the subsequent heat treatment process, the microstructure evolution is a static process, and the energy storage after thermal deformation is further released, resulting in the evolution of grain structures. Three stages of grain structures evolution, i.e., recovery, recrystallization, and grain growth are influenced by deformation parameters, which contributes to the final product performance. Most researches [6−8] focused on the rheological behavior and microstructures during hot deformation, and few studies have linked subsequent heat treatment and consider the evolution law of microstructure evolution during the whole process.

There are several factors affecting the grain structure after heat treatment. One is the recrystallization resistance of the material itself, which requires the design of the element composition and proportion of the material. For example, many studies [9−11] have shown that an appropriate amount of Mn can significantly improve the recrystallization resistance of aluminum alloy, but it requires a lot of experiments to find the most appropriate composition proportion, so as not to affect the mechanical properties or corrosion properties of the alloy. The second one is the heat treatment process. The reports [12, 13] have pointed out that increasing temperature of heat treatment and shortening the time as far as possible will reduce coarse grain structure and achieve the best heat treatment effect. In addition, deformation state of material also affects the microstructure after heat treatment. The driving force of material recrystallization is its internal energy storage, which is related to the deformation state of the material. Therefore, by optimizing the deformation process parameters, the forging can retain the fiber structure to the maximum extent after heat treatment. According to the research of ZENER et al [14], the activation process of strain rate during high temperature plastic deformation is controlled by heating, and the relationship between strain rate and deformation temperature can be expressed by temperature compensated strain rate Z parameter.

Therefore, in the case of the most suitable heat treatment process, this study attempts to establish the relationship between the Z parameter and the grain structure, including recrystallization fraction, grain sizes, local misorientation, geometrically necessary dislocation (GND) and stored strain energy during hot deformation and subsequent heat treatment. Combined with the constitutive equation, the recrystallization mechanism in the whole process is discussed in detail through quasi-in-situ EBSD method, which provides a reference for the actual forging process.

2 Materials and experimental methods

2.1 Isothermal compression experiment

The materials used in thermal simulation are Al-Mg-Si alloy commercial work hardened plates produced in the same batch with sizes of 25 mm× 100 mm×500 mm. Table 1 lists the detailed chemical composition of the materials. As shown in Figure 1, in order to obtain the experimental sample with uniform composition and ensure the consistency among the samples, cylindrical samples with size d10 mm×15 mm were cut perpendicularly to the rolling direction. Since the plate is not heat treated, it needs to be kept at 500 °C for 1 h to remove the internal stress, and then cooled in cold water before hot deformation.

Table 1 Chemical composition of alloy (wt%)

Si	Mg	Mn	Fe	Ti	Zn	Cu	Al
0.917	0.766	0.520	0.216	0.026	0.024	0.011	Bal.

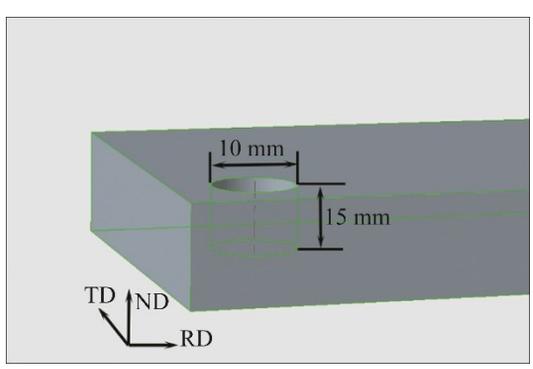

Figure 1 Schematic map of sampling position

Isothermal compression test was conducted on the Gleebe 3500 simulation machine. Before compression, two ends of the samples were coated with 90 vol% oleic acid and 10 vol% paraffin worked as lubricant to reduce the influence of friction. To ensure uniform temperature distribution, the samples were heated to the set temperature at a heating rate of 5 °C/s and held for 3 min before compression. Under strain rates of 0.001, 0.01, 0.1 and 1 s^{-1}, cylindrical specimens were isothermally compressed at 400, 450, 500 and 550 °C. After hot deformation, specimens were quenched into water immediately to maintain the deformed microstructure.

2.2 Subsequent heat treatment and quasi-in-situ microstructure characterization

The deformed samples were cut parallelly to the compression axis along the direction of centerline, and the surface was mechanically ground and polished to 0.5 μm surface roughness. The grain structures of samples were observed by EBSD under the ZEISS EVO MA10 scanning electron microscope. Samples for EBSD characterization were electropolished in a mixed acid solution of 10 vol% $HClO_4$ and 90 vol% C_2H_5OH at 20 V for 10 s at room temperature. In order to obtain quasi-in-situ grain structures during subsequent heat treatment at 550 °C for 1 h, a sharp needle with diameter about 100 μm in SEM was used to position the observation field from the hot deformed samples. After heat treatment, samples were quenched into cold water fast, then electropolished for 10 s at 20 V under −25 ℃. EBSD characterization results indicated that the thickness reduction during re-polishing was less than 1 μm.

The required EBSD data was analyzed through the HKL Channel 5 software. In order to ensure the consistency of data between samples, misorientations below 2° were not measured in this work. In the corresponding EBSD map, the low angle grain boundaries (LAGBs) with grain boundary orientation angle of 2°−15° were marked with white line, and the high angle grain boundaries (HAGBs) with grain boundary orientation angle greater than 15° were marked with black line. All measurements of grain/subgrain size and boundary spacings were obtained as mean linear intercepts.

3 Results

3.1 Mechanical behavior during hot deformation

The true stress−strain curve of Al-Mg-Si alloy at different temperatures and strain rates are presented in Figure 2. At initial stage of deformation, the flow stress increases rapidly. After reaching the peak, the flow stress decreases or remains stable with further increase of plastic strain. According to the existing theory [15], deformation behavior is the result of the competitive process of work hardening and dynamic softening. In the initial stage of deformation, the stored deformation energy and dislocation density increase rapidly, and more stress is needed to make the dislocation move further, and the rheological stress rises rapidly. As the strain increases further, the flow stress remains stable due to softening mechanisms such as dynamic recovery and dynamic recrystallization. The specific softening mechanism needs to be analyzed in combination with the microstructure after deformation, which will be discussed in detail in the following sections. In addition, it can be seen from the flow curve that the thermal deformation temperature and strain rate have a significant influence on the flow performance of Al-Mg-Si alloy. In general, the flow stress levels increase with the decrease of temperature and the increase of strain rate. Their relationship can be expressed by the temperature compensated deformation rate factor Z [16].

3.2 Grain structures evolution under various hot deformation parameters

Figure 3 shows the original microstructure of Al-Mg-Si alloy extracted from thick plate after annealing. Figure 3(a) shows the inverse pole figure (IPF) map overlapped with grain boundaries. What can be drawn from the grain map is that, except for a few small grains at grain boundaries, the main microstructure is strip grain structure with grain spacing of 50 − 100 μm. There are also extensive subgrain structures in large strip grains. These subgrain boundaries are composed of small angle grain boundaries with an orientation of 2°−15°. The distribution of misorientation angle is shown in Figure 3(b). The LAGBs accounts for 69.8%, while

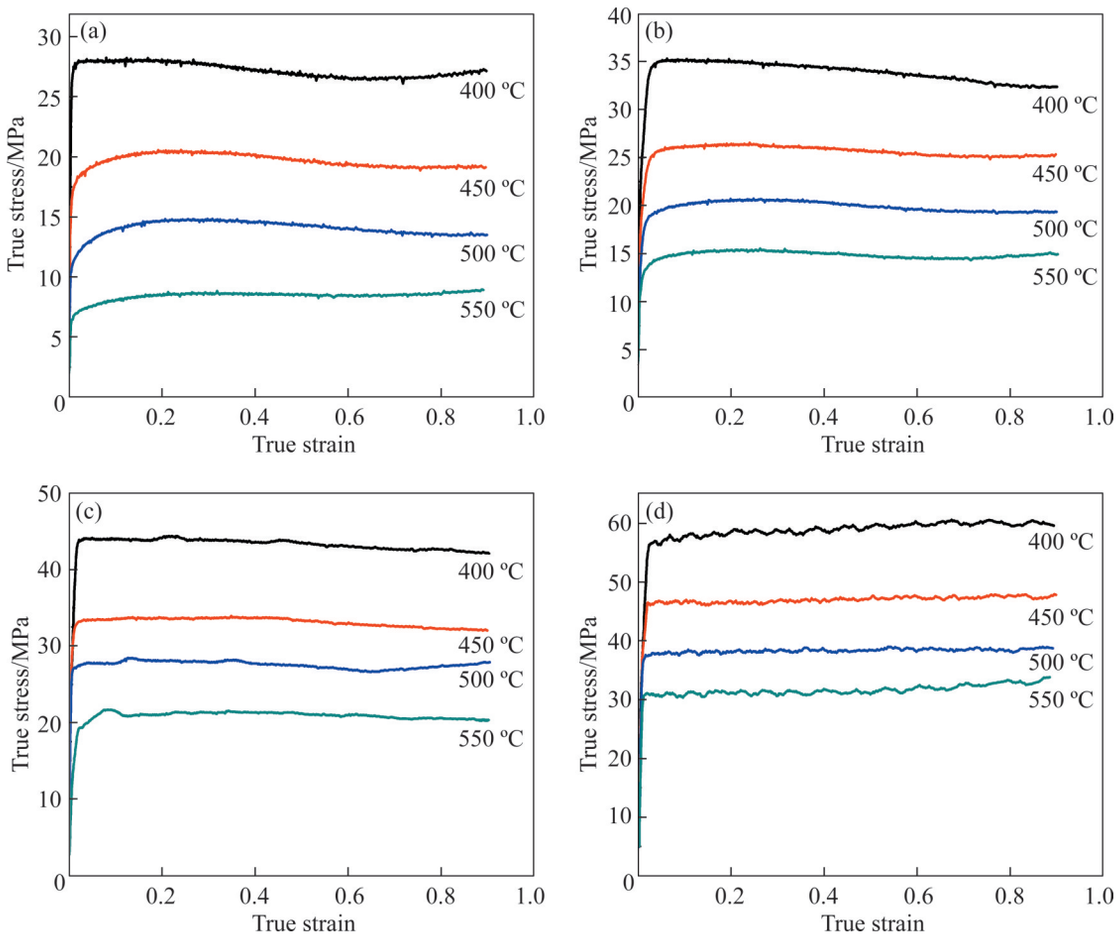

Figure 2 True stress–strain curves of Al-Mg-Si alloy under different conditions: (a) $\dot{\varepsilon}$ =0.001 s^{-1}; (b) $\dot{\varepsilon}$ =0.01 s^{-1}; (c) $\dot{\varepsilon}$ =0.1 s^{-1}; (d) $\dot{\varepsilon}$ =1 s^{-1}

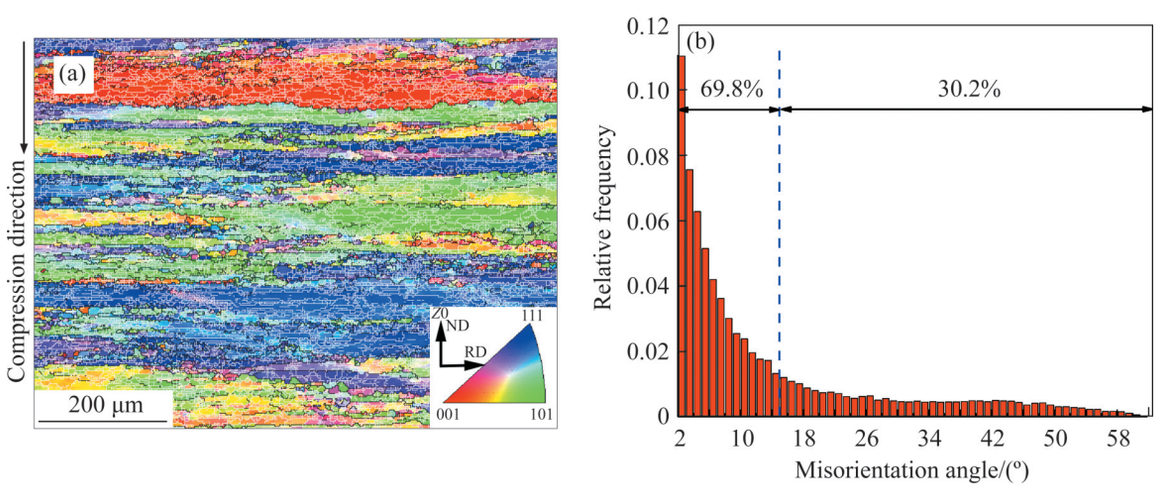

Figure 3 EBSD characterization of original microstructure of Al-Mg-Si alloy: (a) IPF map; (b) Distribution of misorientation angle and boundaries with misorientation lower and higher than 15° (LAGBs and HAGBs)

the HAGBs accounts for 30.2%, indicating that the primary structure sub-grains accounts for the main components.

Figure 4 shows that the microstructure of the alloy changes with temperatures. It can be seen from the IPF maps that the grain structure after isothermal compression can be divided into two types. One is the fiber large grain with width of about 20 μm, which have many subgrains inside. The other one is the equiaxed recrystallized grain

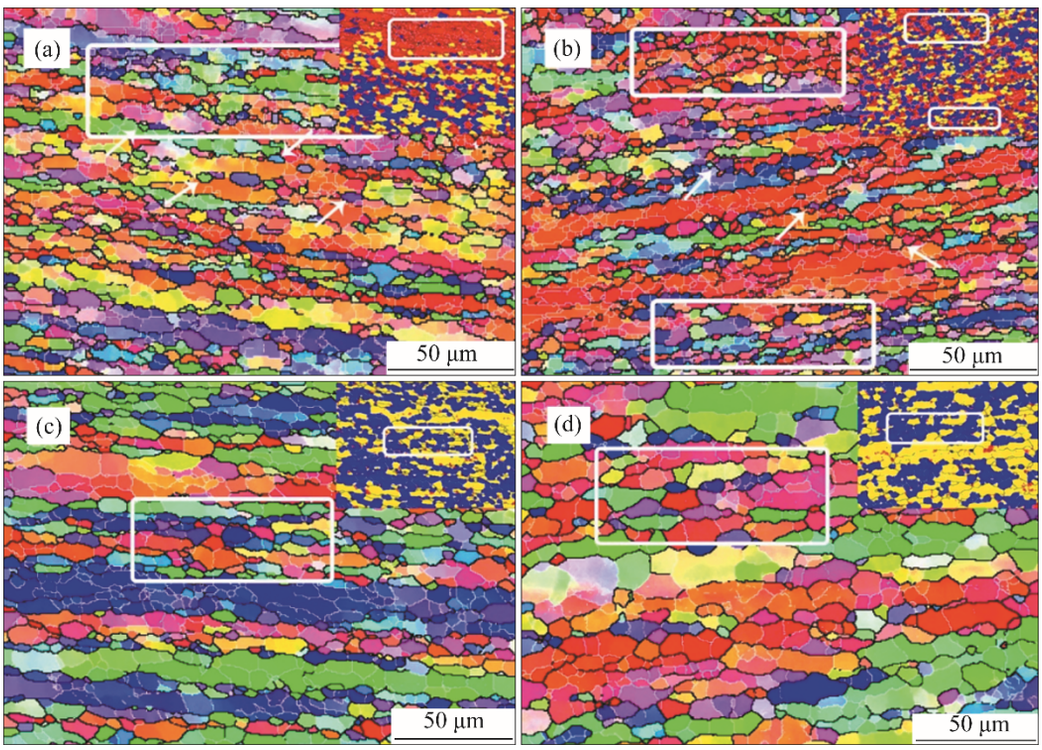

Figure 4 IPF maps and grain orientation spread (GOS) maps of isothermal compression sample at $\dot{\varepsilon}$ =1 s^{-1}: (a) 400 °C; (b) 450 °C; (c) 500 °C; (d) 550 °C (Red region with GOS>7.5 is deformed grain, blue region with GOS<1 is dynamic recrystallization grain, and yellow region with 1<GOS<7.5 indicates a lot of subgrains)

distributed along the grain boundary. Temperature has a great influence on the morphology of these grains. At lower temperature of 400 – 450 °C, the original strip grains are extruded to the fiber grains with only less than two sub-grain's size, and the deformation degree is severe. Many fine equiaxed grains are generated in fiber grains and along the grain boundaries, as shown by the arrow. Overall, the average grain size after hot deformation under 400 – 450 °C is smaller. With the temperature increase to 500 °C, the distribution of fiber grains gets heterogeneous, and both sizes of equiaxed- and sub-grains increase. At 550 °C, the grains can be fully recovered and recrystallized, therefore the grains grow into larger size, and almost all the original strip structures are transformed into equiaxed grains.

It can be seen from GOS maps that at 400 – 450 °C, the deformation is more severe, recrystallized grains, subgrains and deformed structures are mixed together in the sample. All these features marked with white frame are reflected in Figure 4. With the increase of temperature, the recrystallized grains increase obviously, and the deformed structure decreases gradually. At 500 – 550 °C, there is almost no deformed structure, but a large number of recrystallized grains and some subgrains due to the dynamic recrystallization and dynamic recovery.

In addition to the deformation temperature, the strain rate also has a great influence on the grain morphology. As shown in Figure 5, when the strain rate is 10^{-3} s^{-1}, almost all of them are equiaxed recrystallized grains, indicating that at lower strain rate, the work hardening induced by deformation has sufficient time to be offset by the softening mechanism of the alloy, and the recrystallized grains also have sufficient time to grow. With the increase of deformation rate, the recrystallization fraction decreases and the grain size becomes finer. At strain rate of $10^{-2} – 10^{-1}$ s^{-1}, the original grains are mixed with HAGBs and LAGBs, which indicates that the recrystallization appears. When the strain rate is 1 s^{-1}, as shown in Figure 2(d), the dislocation generation rate and the number of barriers to dislocation motion increase. Therefore, the stress required for dislocation motion increases and the flow stress rises. On the other hand, at the early

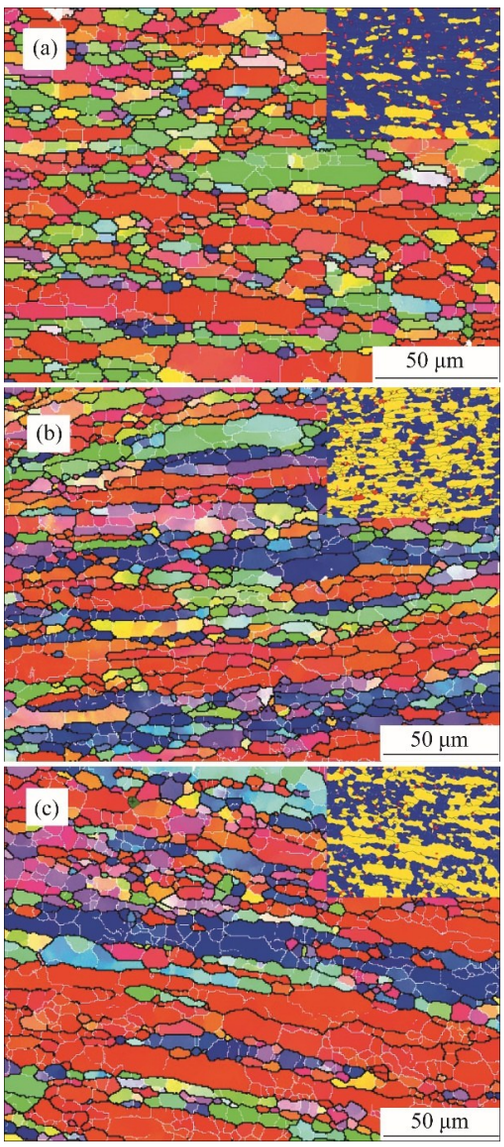

Figure 5 IPF maps and GOS maps of isothermal compression sample at 450 ° C: (a) $\dot{\varepsilon}$ =0.001 s^{-1}; (b) $\dot{\varepsilon}$ =0.01 s^{-1}; (c) $\dot{\varepsilon}$ =0.1 s^{-1}

stage of deformation, the softening effect produced by recovery and recrystallization is not enough to counteract the work hardening caused by deformation, so that the steady state can be achieved at a higher flow stress level. As shown in Figure 4(b), at higher strain rate, there is finer structure mixed with deformed structure and recrystallized grains. Fiber grains formed with width less than two subgrains after compression deformation. At this time the original grain boundaries begin contacting each other at the serrations, causing grain portions to pinch-off, which indicates that geometric dynamic recrystallization (GDRX) will occur at high strain rate. This result is consistent with that reported by CHAMANFAR et al [2].

The EBSD images of the alloy deformed at 450 °C and 0.1 s^{-1} under various strains are displayed in Figure 6. At the initial stage of deformation, dynamic recovery is the main softening mechanism under the action of stress and high temperature. At a strain of ε =0.3, the original large grains are extruded into strips, as shown in Figure 6(a), and there are subgrains which rotate with the increase of misorientation inside the grains. When the true strain increases to 0.5, some of the original grains are reduced into fiber grains with the width of less than two subgrain's size, forming equiaxed grains with the same size as the subgrains (as shown in black frames in Figures 6(b) and (c)). This phenomenon indicates that GDRX may occur at this time [17]. As the strain increased from ε=0.7 to ε=1.1, the grain structure remains stable, which is the result of dynamic equilibrium between dynamic softening and work hardening.

3.3 Grain structures evolution during subsequent heat treatment

In order to study the grain structures evolution of samples during subsequent heat treatment after hot deformation, samples with different thermal deformation conditions were investigated. Both discontinuous and continuous static recrystallization occurs during heat treatment, as observed in Figure 7. After hot deformed at 450 °C and 0.1 s^{-1}, the deformed sample performed discontinuous recrystallization during heating at 550 °C for 1 h, as indicated by the EBSD result in Figure 7(c) compared with Figure 7(a). During this process, abnormal grain growth occurs, and the fractions of both recrystallization and subgrains significantly increase. As shown in Figures 7(g) and (h), there are much more large grains produced by discontinuous recrystallization after heat treatment at low temperature and high strain rate. It shows that some dislocations form LAGBs due to static recovery, and more subgrains indicate that abnormal grains are easier to form.

Compared with Figure 7(b), after hot deformation at 450 ℃ and 0.01 s^{-1}, there are obvious subgrains merging and disappearing and some

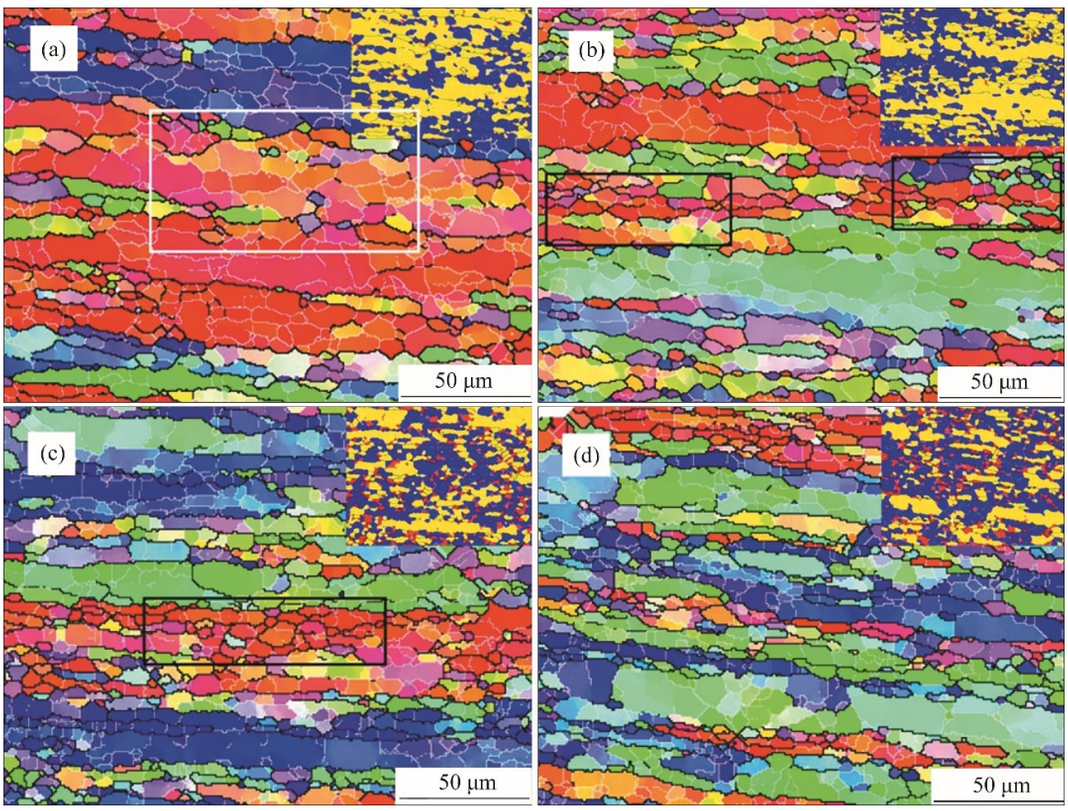

Figure 6 EBSD images with different deformations at 450 °C and 0.1 s^{-1}: (a) ε=0.3; (b) ε=0.5; (c) ε=0.7; (d) ε=1.1

grains growing up during subsequent heating at 550 °C for 1 h, indicating that only continuous recrystallization occurs, as shown in Figure 7(e). This is also demonstrated by the significant decrease in LAGBs shown in the misorientation distribution in Figure 7(i).

For the hot deformation at 500 °C and 0.01 s^{-1}, after the same heat treatment, only sub grains merge and disappear, but the change of grain size is not obvious, as compared with the EBSD result in Figures 7(c)− (f). Compared with the previous two hot deformation states, the grain structure is more stable due to the release of deformation energy, which can also be proved from the distribution of misorientation in Figure 7(i). In the following section, the recrystallization mechanism will be revealed by quantitative analysis of samples under different deformation conditions.

4 Discussion

4.1 Mechanical modelling of hot deformation process

At present, the commonly applicable constitutive equation is the hyperbolic sine Arrhenius equation proposed by SELLARS et al [18]. The equation includes the influence factors of strain rate $\dot{\varepsilon}$, deformation temperature T and deformation activation energy Q. The expression can be expressed by

$$\dot{\varepsilon} = AF(\sigma)\exp\left(-\frac{Q}{RT}\right) \tag{1}$$

It can be seen from Eq. (1) that the strain or steady state stress σ in any state is affected by the strain rate $\dot{\varepsilon}$ and deformation temperature T during the thermal deformation of materials. Among them, $F(\sigma)$ is the expression function of stress [19]. According to different stress levels, there are three kinds of mathematical expressions between σ, $\dot{\varepsilon}$ and T, which are:

$$\begin{cases} \dot{\varepsilon} = A_1\sigma^{n_1}\exp\left(-\dfrac{Q}{RT}\right), & \alpha\sigma < 0.8 \\ \dot{\varepsilon} = A_2\exp(\beta\sigma)\exp\left(-\dfrac{Q}{RT}\right), & \alpha\sigma > 1.2 \\ \dot{\varepsilon} = A_3\left[\sinh(\alpha\sigma)\right]^n\exp\left(-\dfrac{Q}{RT}\right), & \text{for all } \sigma \end{cases} \tag{2}$$

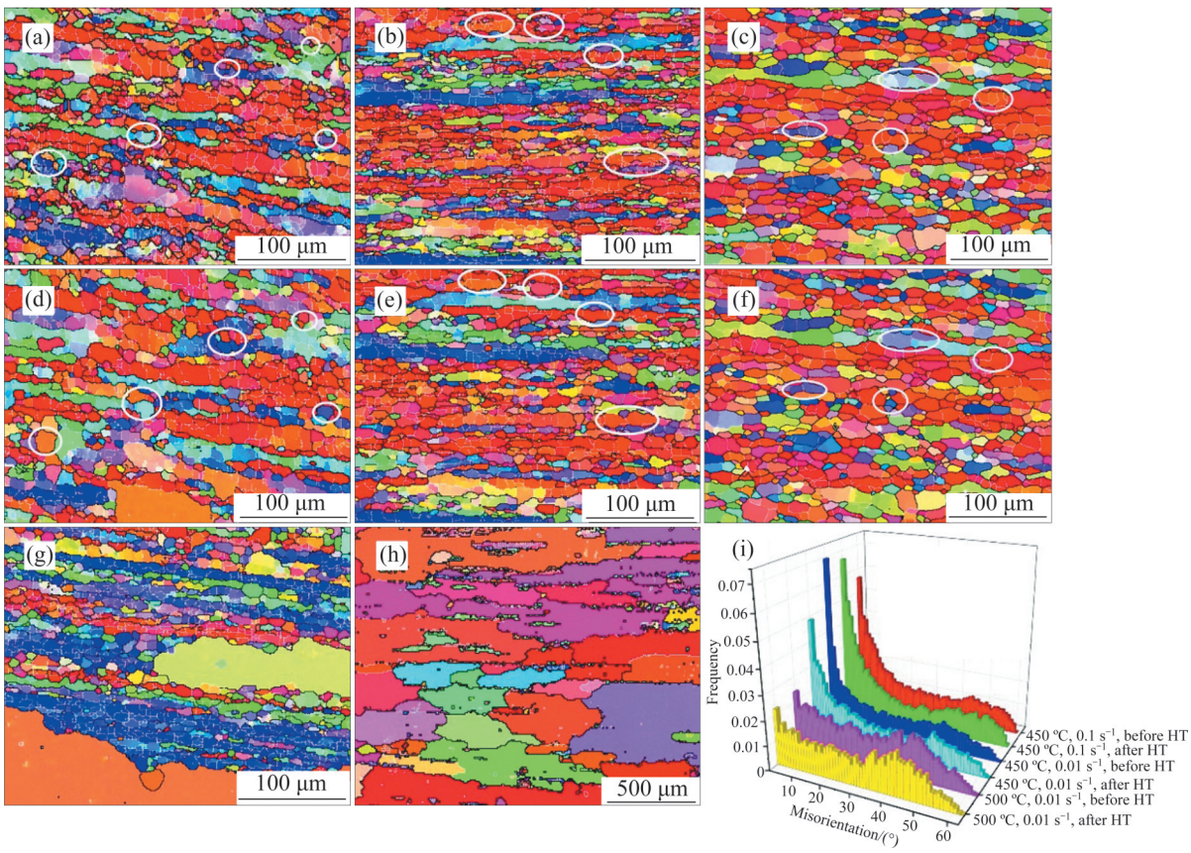

Figure 7 IPF maps and GOS maps: (a) 450 °C, 0.1 s^{-1} before HT; (b) 450 °C, 0.01 s^{-1} before HT; (c) 500 °C, 0.01 s^{-1} before HT; (d) 450 °C, 0.1 s^{-1} after HT; (e) 450 °C, 0.01 s^{-1} after HT; (f) 500 °C, 0.01 s^{-1} after HT; (g) 450 °C, 1 s^{-1} after HT; (h) 400 °C, 1 s^{-1} after HT; (i) Misorientation of 450 °C, 0.1 s^{-1}, 450 °C, 0.01 s^{-1} and 500 °C, 0.01 s^{-1} before and after HT

where A_1, A_2, A_3, n_1, α and β are material constants independent of deformation temperature, and $\alpha = \beta/n_1$, and R is the universal gas constant (8.3145 $J \cdot mol^{-1} \cdot K^{-1}$). In order to calculate the above materials constants, the natural logarithm is taken on both sides of Eq. (2):

$$\begin{cases} \ln \dot{\varepsilon} = \ln A_1 + n_1 \ln \sigma - \dfrac{Q}{RT} \\ \ln \dot{\varepsilon} = \ln A_2 + \beta\sigma - \dfrac{Q}{RT} \\ \ln \dot{\varepsilon} = \ln A - \dfrac{Q}{RT} + n \ln\left[\sinh(\alpha\sigma)\right] \end{cases} \tag{3}$$

It can be seen from Eq. (3) that when the deformation temperature T is constant, $\ln \dot{\varepsilon} - \ln \sigma$ and $\ln \dot{\varepsilon} - \sigma$ show linear relationship. Take the steady state stress (ε =0.6) as an example to build the constitutive relationship, the values of n_1 and β are obtained from the slopes of the fitting lines $\ln \dot{\varepsilon} - \ln \sigma$ and $\ln \dot{\varepsilon} - \sigma$ as shown in Figures 8(a) and (b), α can be calculated by taking the average value of β/n_1. Similarity, the constant of n can be determined using the slope of the plot of $\ln \dot{\varepsilon} - \ln\left[\sinh(\alpha\sigma)\right]$ as shown in Figure 8(c). The activation energy of hot deformation can be expressed as:

$$Q = Rn \frac{\partial \ln\left[\sinh(\alpha\sigma)\right]}{\partial (1/T)} \tag{4}$$

As shown in Figure 8(d), the relationship between deformation temperature T and flow stress σ can well satisfy Arrhenius relationship, which indicates that the hot deformation behavior of Al-Mg-Si aluminum alloy is controlled by thermal activation energy. By substituting fitting slope values from Figure 8 into Eq. (4), the average activation energy (Q) can be determined from the plot of $\ln\left[\sinh(\alpha\sigma)\right] - 1000/T$, the value of which is 171.91 kJ/mol.

As mentioned above, the relationship between deformation temperature T and strain rate $\dot{\varepsilon}$ can be

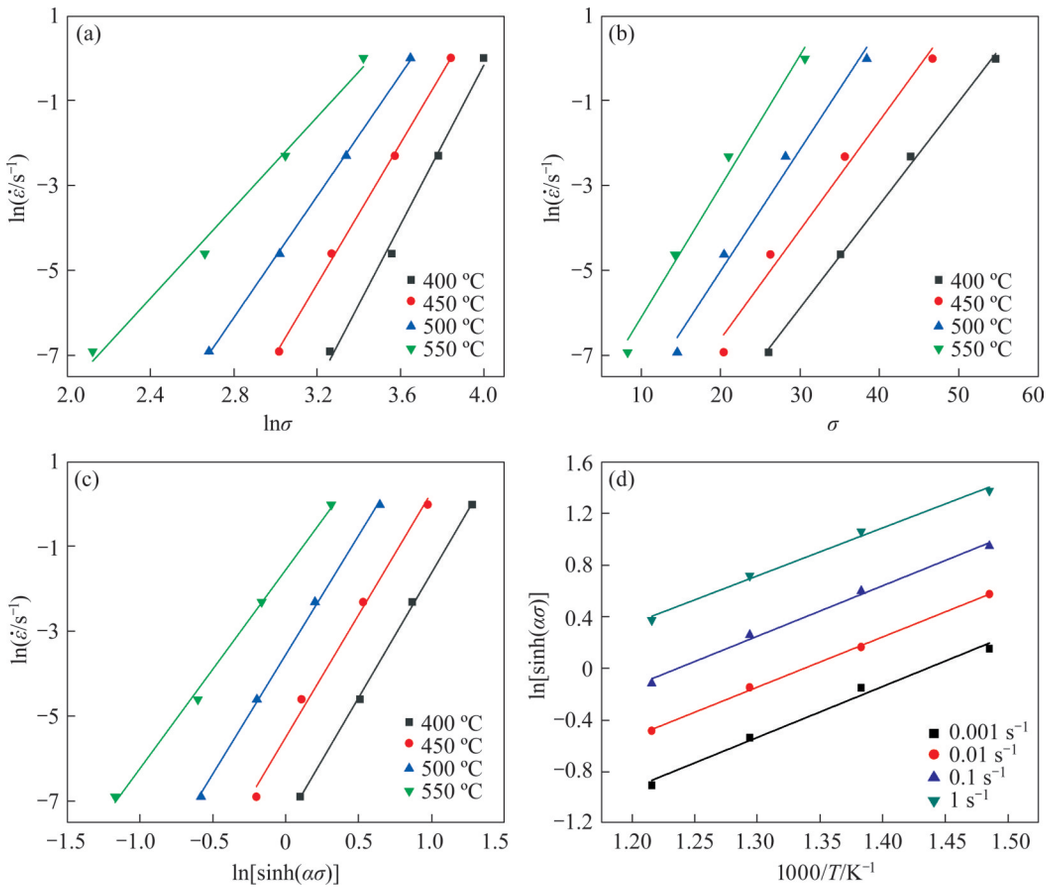

Figure 8 Relationship between $\ln \dot{\varepsilon}$ and $\ln \sigma$ (a), $\ln \dot{\varepsilon}$ and σ (b), $\ln \dot{\varepsilon}$ and $\ln[\sinh(\alpha\sigma)]$(c), $\ln[\sinh(\alpha\sigma)]$ and $1000/T$ (d)

expressed by the following formula:

$$Z = \dot{\varepsilon}\exp\left(\frac{Q}{RT}\right) = A[\sinh(\alpha\sigma)]^n \tag{5}$$

By substituting Q value determined above, Z parameters under various hot compression conditions can be calculated [20]. Z is Zener-Hollomon parameter, which is used to correlate deformation temperature and strain rate with flow stress when the strain is 0.6. As shown in Figure 9, all the experimental data are kept on the same line, and the flow stress increases with the increase of Z parameter, and its correlation can be expressed as Eq. (10).

$$\sigma = \frac{1}{\alpha}\operatorname{arc\,sinh}\left[\left(\frac{z}{A}\right)^{\frac{1}{n}}\right] = \frac{1}{\alpha}\ln\left\{\left(\frac{Z}{A}\right)^{\frac{1}{n}} + \left[\left(\frac{Z}{A}\right)^{\frac{2}{n}} + 1\right]^{\frac{1}{2}}\right\} \tag{6}$$

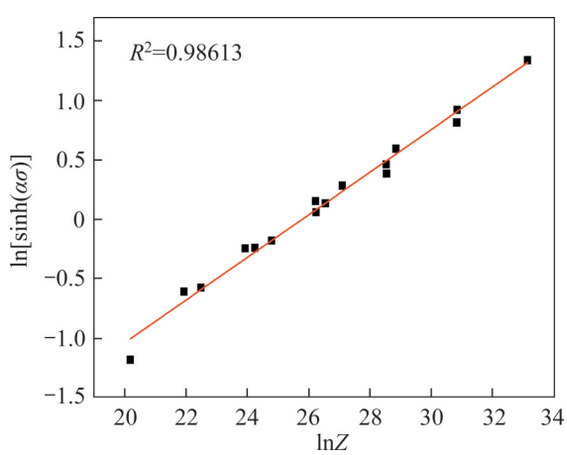

Figure 9 Variation of flow stress at strain of 0.6 as a function of Z parameter for Al-Mg-Si alloy

4.2 Effect of stored energy on microstructure evolution

In order to quantitatively analyze the microstructure evolution during hot deformation and subsequent heat treatment, the variation trend of HAGB and the volume fraction of recrystallized grains was counted based on the data of EBSD, as shown in Figure 10. It is obvious that the recrystallization fraction and HAGB decrease with the increase of Z during hot deformation. As discussed before, decreasing Z value, which is equal

to increasing deformation temperature or decreasing strain rate, leads to more adequate proceeding of DRX because of high driving force and sufficient time for recrystallization. In addition, both recrystallization fraction and HAGB can establish a linear relationship with ln$Z$, which is:

$$V_{DRX}=-4.69\ln Z+180.59 \quad (7)$$

$$V_{HAGB}=-0.15\ln Z+118.65 \quad (8)$$

After heat treatment, it is evident that two kinds of recrystallization have occurred, as shown in Figure 11. When ln$Z$< 28, the continuous recrystallization process is similar to the hot deformation process, because recrystallization fraction and V_{HAGB} are still linear with ln$Z$. The difference is that the recrystallization fraction increases slightly, while the V_{HAGB} decreases. The former is due to the occurrence of SRX, most of the deformation energy storage can be released at low ln$Z$, so the heat treatment process has little change. The latter is due to the growth of some small grains and polygonization of partial residual dislocations, as shown in Figure 7, resulting in the decrease of V_{HAGB}. When the ln$Z$ increases to higher than 28, discontinuous recrystallization occurs with the growth of abnormal grains, the recrystallization fraction and V_{HAGB} increase rapidly, which may be due to the greater energy storage and the easier growth of abnormal grains.

When ln$Z$=28, the value of V_{HAGB} is about 60%, which is consistent with the results of other researchers [21 − 23]. HUMPHREY's results [22] showed that there is a transition from continuous to discontinuous at the critical value of V_{HAGB} and low angle subgrain microstructures are predicted to be intrinsically unstable with respect to discontinuous subgrain growth. JAZAERI et al [21] also found that no continuous recrystallization occurred when V_{HAGB}<62% and no discontinuous recrystallization when HAGB% >64%. He believed that the higher energy and mobility of low angle grain boundary is the main reason for discontinuous recrystallization.

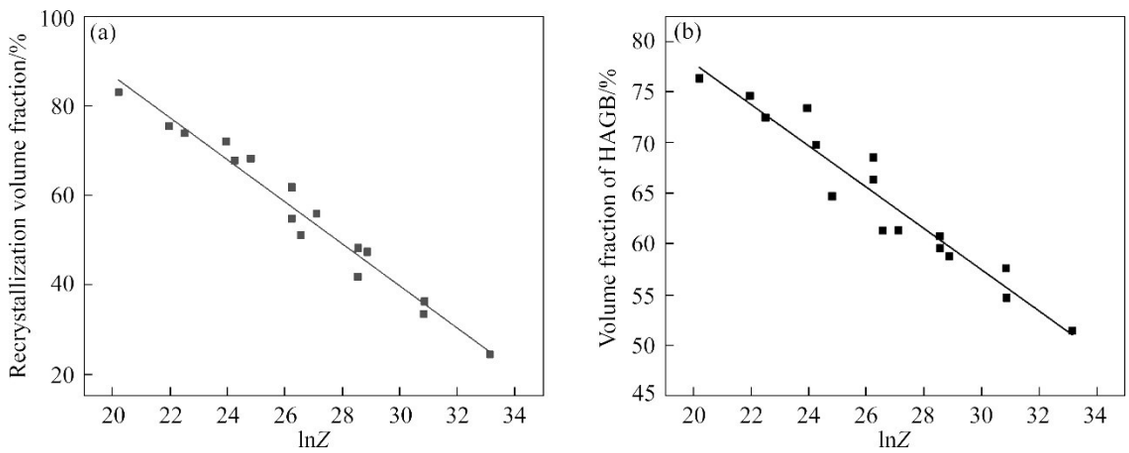

Figure 10 Recrystallization fraction (a) and HAGBs fraction (b) change with ln$Z$ before heat treat went

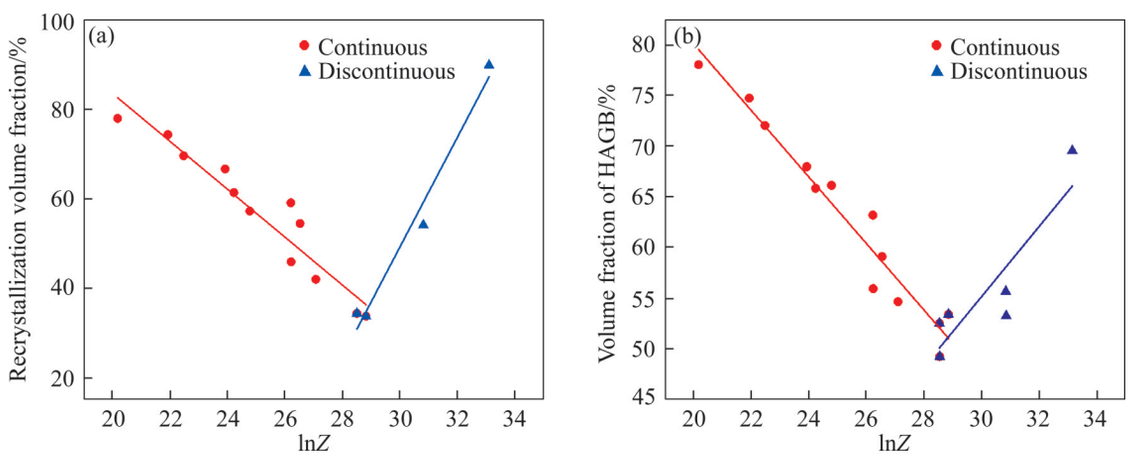

Figure 11 Recrystallization fraction (a) and HAGBs fraction (b) change with ln$Z$ after heat treat went

According to the results summarized above, as shown in Figure 12(a), we can obtain the boundary between continuous and discontinuous recrystallization. This phenomenon is also reflected in the average (sub)grain size and energy storage. The dependency of the average (sub)grain size on the ln$Z$ value is depicted in Figure 12(b), and the relationship is

$$\frac{1}{D} = a_1 + b_1 \ln Z \tag{9}$$

The reciprocal of (sub)grain size is linearly related to ln$Z$, that is, the average (sub)grain size decreases with the increase of ln$Z$. This behavior can be attributed to the decrease of deformation temperature and the increase of strain rate, i.e. with the increase of ln$Z$ value, the growth rate of recrystallized grains slows down and the migration time of subgrain boundary decreases. So, smaller grain size was attained at higher ln$Z$ value.

However, in the process of subsequent heat treatment, the relationship changes to

$$\frac{1}{D} = a_2 + b_2 \ln Z + c(\ln Z)^2 \tag{10}$$

Similarly, when the value of ln$Z$ is close to 28, the grain size shows the boundary between discontinuity and continuous recrystallization. This may be due to the worse stability of fine grains, when ln$Z$ > 28, abnormal grains are more likely to appear driven by higher energy storage after heat treatment. Figure 11 also proves that the material has good stability during heat treatment at lower ln$Z$ values. In addition, the error bars in the measurement of grain and (sub)grain sizes in Figure 12(b) can be attributed to fairly heterogeneous microstructure and changes in (sub) grain structures between different regions.

The geometric dislocation density plays an important role in the recrystallization during hot deformation and subsequent heat treatment. Geometric dislocation density could be represented via the misorientation between a data point and its neighbors by the kernel average misorientation (KAM) method. In this method, the misorientation is equal to the average misorientation between the analysis point located at the center of the kernel and all its neighboring points on the perimeter of the kernel, which is calculated with the proviso that misorientations exceeding a tolerance value of 5° are excluded from averaging calculation [24, 25]. The KAM distributions of hot deformed specimens with different temperatures and strain rates are presented in Figure 13. It is obvious that the orientation gradient decreases with the increase of temperature and the decrease of strain rate. There are few orientation gradient differences in samples with the same ln$Z$, which indicates that the deformation stored energy of materials has a certain correlation with ln$Z$. Figure 14 shows the KAM diagram of samples with different ln$Z$ after heat treatment. At higher ln$Z$, the orientation gradient of the sample decreases sharply due to discontinuous recrystallization. However, at low ln$Z$, the orientation gradient of the sample changes little. Quantitative analysis will be carried out below.

As a first-order approach, the KAM which is calculated from EBSD data was chosen as a

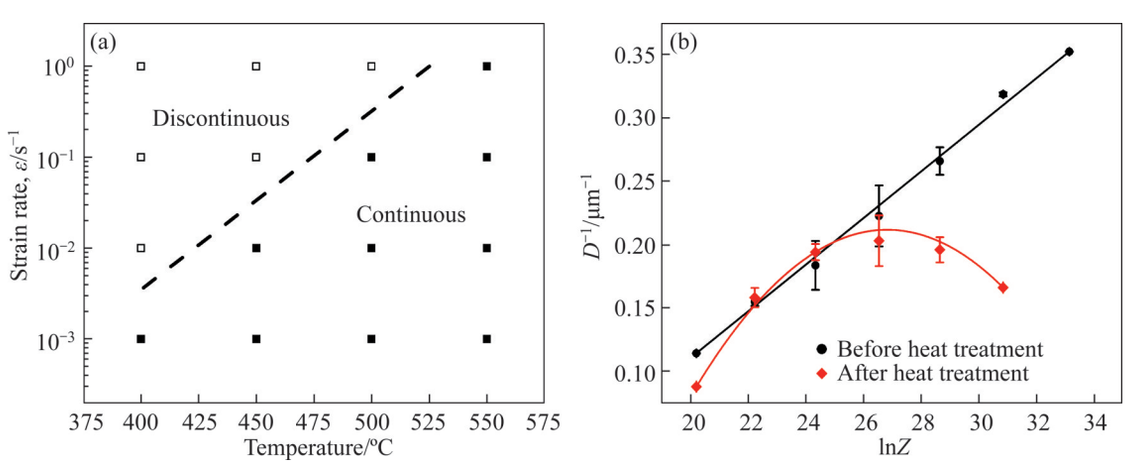

Figure 12 Effect of temperature and strain rate on transition from continuous to discontinuous recrystallization after heat treatment (a) and (sub)grain size change with ln$Z$

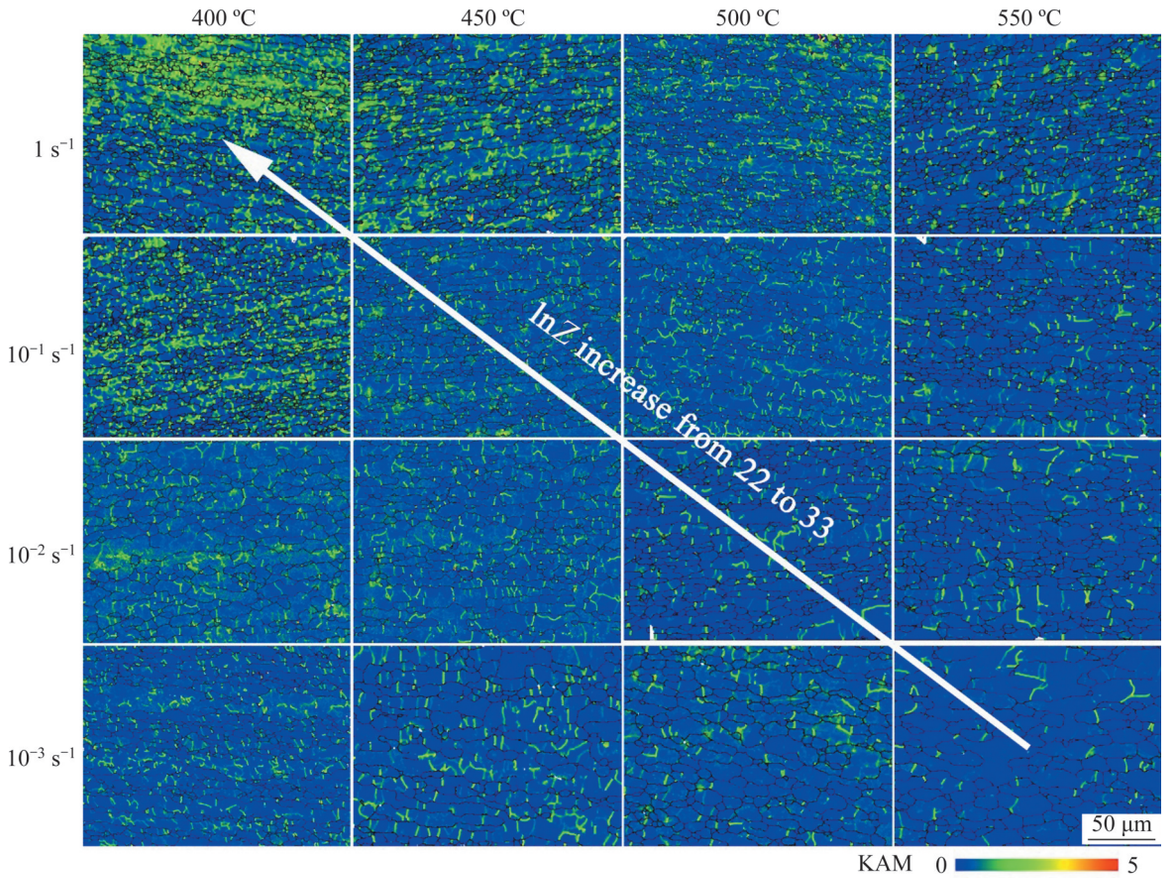

Figure 13 KAM map of thermal deformed samples under different parameters

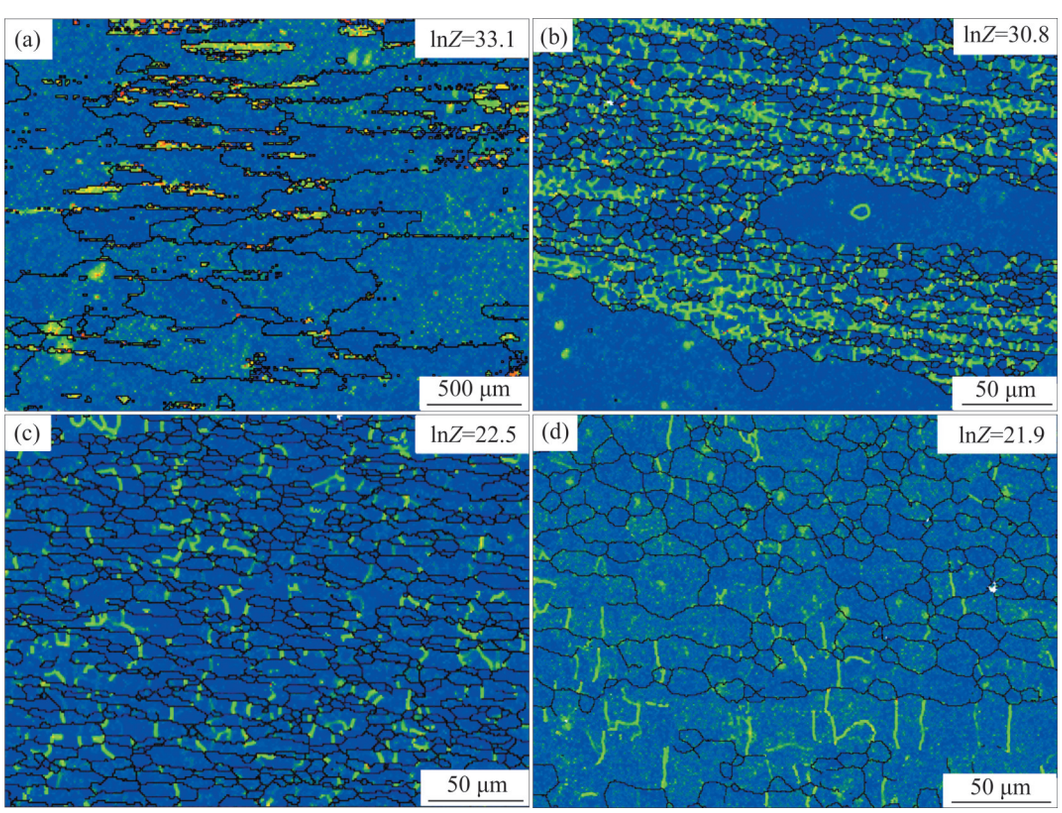

Figure 14 KAM maps of samples under different parameters after HT: (a) 400 °C, 1 s^{-1}; (b) 450 °C, 0.1 s^{-1}; (c) 500 °C, 10^{-3} s^{-1}; (d) 550 °C, 10^{-2} s^{-1}

measure used to calculate GND densities [24], though it should be underestimated because of existence of dislocations that do not contribute nor build up the misorientation. From the KAM value, the GND density ρ can be derived as [26, 27]

$$\rho \approx \frac{\alpha\theta}{bd} \tag{11}$$

where θ is the average misorientation angle across the dislocation boundaries, which can be derived from KAM value; b is the magnitude of the Burgers vector, which is 0.286 nm for aluminum; d is the distance between the misoriented points, namely the step size of the EBSD map, which is fixed at 0.8 μm in the present study; constant α is dependent on the nature of dislocations edge or screw, and α=3 was proposed [28]. The GND density ρ obtained from Eq. (11) can be used as a reference value to reflect the real dislocation density. The stored strain energy per unit volume (E) can be obtained by the following equation.

$$E = \frac{1}{2}\rho G b^2 \tag{12}$$

where G is the shear modulus and 26.1 GPa for an aluminum. For a more quantitative comparison, the values of ρ and E before and after heat treatment are presented in Figure 15. It is noted that the calculated values of the above parameters are increased with increasing ln$Z$ before heat treatment, and the relationship is

$$\rho_{GND}=0.1087\ln Z-1.7012, \text{ before heat treatment} \tag{13}$$

$$\rho_{GND}=0.0558\ln Z-0.5553, \text{ after heat treatment} \tag{14}$$

Similarly, the relationship between dislocation density and energy storage is linear with ln$Z$ during hot deformation and subsequent heat treatment, which indicates that continuous recrystallization process occurred in both processes. After heat treatment, the slope decreases from 0.1087 to 0.0558. With higher ln$Z$, the dislocation density declines much sharply. When ln$Z$<28, dislocation density becomes more stable with less reduction during subsequent heat treatment after hot deformation. As these dislocations distributed along LAGBs, the subgrain has good stability during subsequent heat treatment.

4.3 Recrystallization mechanism before and after heat treatment

Figures 4−6 briefly describes the microstructure evolution during hot deformation from three aspects of temperature, strain rate and deformation amount. However, the specific recrystallization mechanism and the change of recrystallization mode during subsequent heat treatment need to be analyzed in combination with individual grain orientation and KAM diagram.

Enlarge the white marking area of Figure 6(c), as shown in Figure 16(a), some isolated high angle grain boundaries can be observed inside the original grains, and the misorientation of these grain boundaries is between 15° and 20° which indicates that these high angle grain boundaries are newly formed and transformed from low angle grain boundaries. It can be observed that some recrystallized grains are distributed along original grain boundaries, and the misorientations between the recrystallized grains and the surrounding grains are 30° − 50°, which indicates that those subgrains

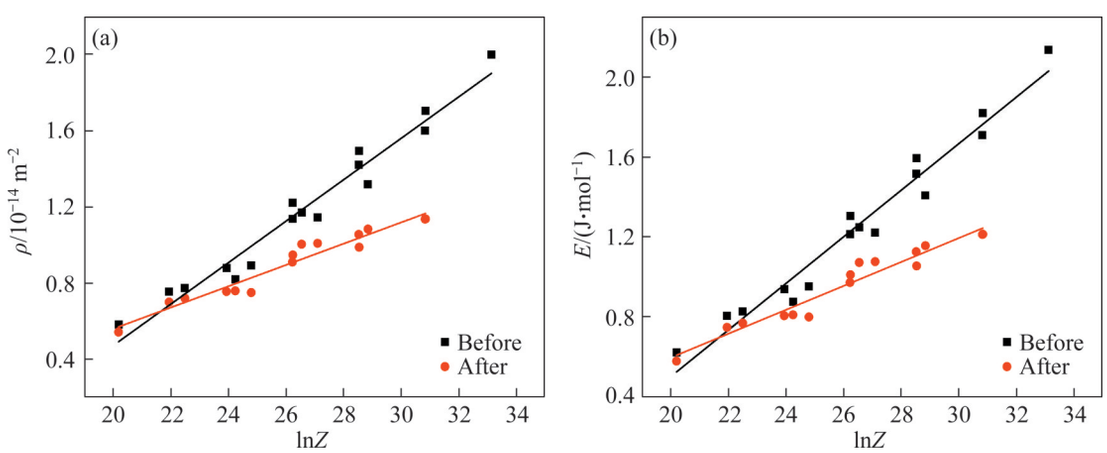

Figure 15 Relationships between dislocation density (a) and energy storage (b) with ln$Z$ before and after heat treatment

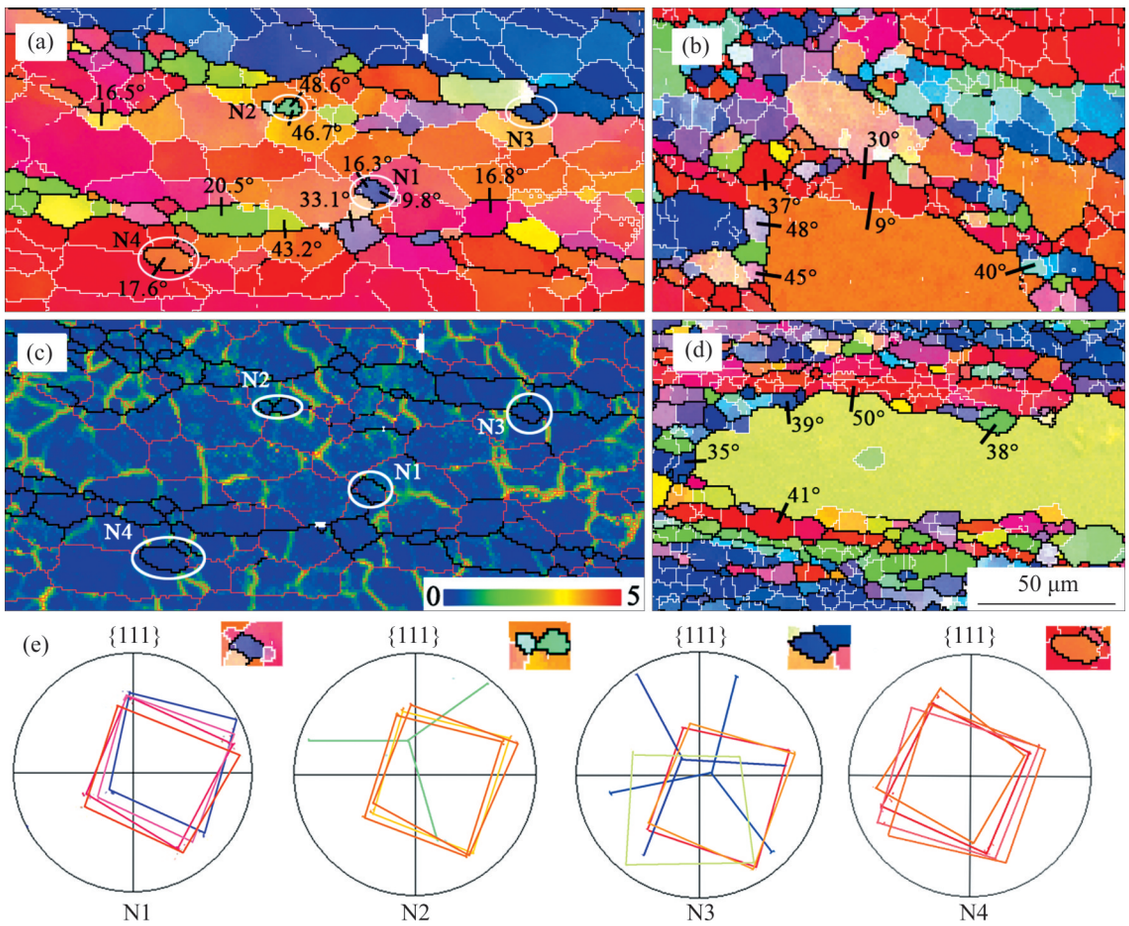

Figure 16 (a) IPF map when true strain is 0.3; (b) Region of discontinuous recrystallization at 450 °C and 0.1 s^{-1} after HT; (c) KAM map; (d) Region of discontinuous recrystallization at 450 °C and 1 s^{-1} after HT; (e) Orientation relationship between four new recrystallized nuclei (N1, N2, N3, N4) and surrounding grains on {111} pole figures

near the grain boundaries are easier to transform into high angle grain boundaries due to their higher potential energy. Moreover, the KAM map can be used to describe the dislocation density or degree of strain in the grains. As shown in Figure 14(c), the deformed recrystallized grains and the newly formed recrystallized grains can be distinguished from the KAM map. The {111} polar figures of newly formed recrystallized nuclei are shown in Figure 16(e). These nuclei can be divided into two types. One type has similar orientations with the surrounding grains, such as N1 and N4, which are formed inside the large grains, indicating that they are formed by the rotation of subgrains. Another type is far away from 40° misorientation relationship, such as N2 existing inside original grains and N3 existing at grain boundaries. The recrystallization nuclei inside the large grains may be formed by the extrusion of other original grains, while the nuclei at the grain boundaries grow into the deformed matrix on the other side of the grain boundary through the subgrains on one side of the pre-existing grain boundaries, indicating that continuous dynamic recrystallization (CDRX) is the main softening mechanism.

After heat treatment, the physical mechanisms responsible for dynamic recrystallization (DRX) are similar in many respects to those controlling static recrystallization (SRX). As shown in the white circle in Figure 7, according to the in-situ EBSD results, it can be clearly seen that the reduction of subcrystal in some regions and the growth of recrystallized grains during continuous recrystallization can be seen. However, due to the lack of drive force (deformation stored energy), the grain growth is uniform and continuous. It can be seen from Figures 16(b) and (d) that the abnormal grains, which have an misorientation of 40° with the

surrounding grains, occur at the place with the highest degree of deformation. In the process of grain growth, the HAGBs wipe out the non-recrystallized strained matrix to eliminate the crystal defects until the recrystallized grains collide with each other, which can be performed continuous (normal grain growth, i.e. primary recrystallization) or discontinuous (abnormal grain growth, i. e. secondary recrystallization) recrystallization. For Al alloys, the main factors affecting the grain growth process are the temperature of heat treatment and the interface energy of the material. It is generally believed that the grain boundary tends to protrude to the area with high dislocation density [29]. At this time, the grains grow rapidly in the way of grain boundary migration on the basis of the original grain boundary.

5 Conclusions

In this study, the hot deformation behavior of Al-Mg-Si alloy at temperature of 400−550 °C and strain rate of $1-10^{-3}\ s^{-1}$ was studied by isothermal compression. The microstructure evolution of the materials before and after heat treatment was observed and quantitatively elucidated via quasi-in-situ EBSD technique.

1) The flow stress is related to deformation temperature and strain rate. The stress level decreases with the increase of deformation temperature and the decrease of strain rate. According to the experimental data, the constitutive relation is established, and the activation energy of hot deformation is 171.91 kJ / mol.

2) Through microstructure analysis, the empirical formula between recrystallization fraction, HAGB, grain size, dislocation density and ln$Z$ are summarized. After heat treatment, it is found that there is a transition from continuous to discontinuous near the critical value ln$Z$ equal to 28. Therefore, the coarse grains produced by discontinuous recrystallization can be reduced by adjusting the deformation parameters.

3) During hot deformation, the main recrystallization mechanism is CDRX, accompanied by GDRX at higher ln$Z$. After heat treatment, the mechanism of continuous recrystallization is similar to that of heat treatment. Grain growth in the discontinuous recrystallization process is in the form of grain boundary migration driven by stored energy.

Contributors

LI Ze-cheng's contributions are formal analysis, investigation, writing original draft, software and data curation. DENG Yun-lai's contributions are conceptualization, funding acquisition and project administration. YUAN Man-fa's contributions are formal analysis and supervision. ZHANG Jin's contributions are project administration and resources. GUO Xiao-bin's contributions are methodology, writing review, editing and validation.

Conflict of interest

LI Ze-cheng, DENG Yun-lai, YUAN Man-fa, ZHANG Jin and GUO Xiao-bin declare that they have no conflict of interest.

References

[1] BERGSMA S C, KASSNER M E, LI X, WALL M A. Strengthening in the new aluminum alloy AA 6069 [J]. Materials Science and Engineering: A, 1998, 254 (1): 112−118. DOI: 10.1016/S0921-5093(98)00701-1.

[2] CHAMANFAR A, ALAMOUDI M T, NANNINGA N E, MISIOLEK W Z. Analysis of flow stress and microstructure during hot compression of 6099 aluminum alloy (AA6099) [J]. Materials Science and Engineering A, 2019, 743: 684−696. DOI: 10.1016/j.msea.2018.11.076.

[3] POLETTI C, RODRIGUEZ-HORTALÁ M, HAUSER M, SOMMITSCH C. Microstructure development in hot deformed AA6082 [J]. Materials Science and Engineering A, 2011, 528 (6): 2423−2430. DOI: 10.1016/j.msea.2010.11.048.

[4] ROLLETT A D, KOCKS U F. A review of the stages of work hardening [J]. Solid State Phenomena, 1993, 35, 36: 1−18. DOI: 10. 4028/www.scientific.net/SSP.35-36.1.

[5] MCQUEEN H J. Development of dynamic recrystallization theory [J]. Materials Science and Engineering A, 2004, 387−389: 203−208. DOI: 10.1016/j.msea.2004.01.064.

[6] LIN Y C, CHEN X M. A critical review of experimental results and constitutive descriptions for metals and alloys in hot working [J]. Materials & Design, 2011, 32 (4): 1733−1759. DOI: 10.1016/j.matdes.2010.11.048.

[7] SHI L, YANG H, GUO L G, ZHANG J. Constitutive modeling of deformation in high temperature of a forging 6005A aluminum alloy [J]. Materials & Design, 2014, 54: 576−581. DOI: 10.1016/j.matdes.2013.08.037.

[8] KE B, YE L, TANG J, ZHANG Y, LIU S, LIN H, DONG Y, LIU X. Hot deformation behavior and 3D processing maps of AA7020 aluminum alloy [J]. Journal of Alloys and Compounds, 2020, 845: 156113. DOI: 10.1016/j. jallcom. 2020.156113.

[9] HU R, OGURA T, TEZUKA H, SATO T, LIU Q. Dispersoid formation and recrystallization behavior in an Al-Mg-Si-Mn Alloy [J]. Journal of Materials Science & Technology, 2010, 26 (3): 237−243. DOI: 10.1016/S1005-0302(10)60040-0.

[10] RAKHMONOV J, LIU K, ROMETSCH P, PARSON N, CHEN X G. Effects of Al(MnFe)Si dispersoids with different sizes and number densities on microstructure and ambient/elevated-temperature mechanical properties of extruded Al–Mg–Si AA6082 alloys with varying Mn content [J]. Journal of Alloys and Compounds, 2020: 157937. DOI: 10.1016/j.jallcom.2020.157937.

[11] QIAN X, PARSON N, CHEN X G. Effects of Mn content on recrystallization resistance of AA6082 aluminum alloys during post-deformation annealing [J]. Journal of Materials Science & Technology, 2020, 52: 189−197. DOI: 10.1016/j.jmst.2020.04.015.

[12] MRÓWKA-NOWOTNIK G, SIENIAWSKI J. Influence of heat treatment on the microstructure and mechanical properties of 6005 and 6082 aluminium alloys [J]. Journal of Materials Processing Technology, 2005, 162−163: 367−372. DOI: 10.1016/j.jmatprotec.2005.02.115.

[13] MUKHOPADHYAY P. Alloy designation, processing, and use of AA6XXX series aluminium Alloys [J]. ISRN Metallurgy, 2012, 2012: 1−15 . DOI: 10.5402/2012/165082.

[14] ZENER C, HOLLOMON J H. Effect of strain rate upon plastic flow of steel [J]. Journal of Applied Physics, 1944, 15(1): 22−32. DOI: 10.1063/1.1707363.

[15] HUANG Y, HUMPHREYS F J. Transient dynamic recrystallizationin an aluminium alloy subjected to large reductions in strain rate [J]. Acta Metallurgica, 1997, 45(11): 4491−4503. DOI: 10.1016/S1359-6454(97)00140-7.

[16] JIANG W G, WANG G C, LU S Q, LI J W. Prediction of microstructure evolution of A1-1% Mg alloy during hot forming and sequential heat treatment [J]. Journal of Materials Processing Technology, 2006, 182 (1−3): 274−280. DOI: 10.1016/j.jmatprotec.2006.08.005.

[17] PARI L D, MISIOLEK W Z. Theoretical predictions and experimental verification of surface grain structure evolution for AA6061 during hot rolling [J]. Acta Materialia, 2008, 56 (20): 6174−6185. DOI: 10.1016/j.actamat.2008.08.050.

[18] SELLARS C M, MCTEGART W J. On the mechanism of hot deformation [J]. Acta Metallurgica, 1966, 14(9): 1136−1138. DOI: 10.1016/0001-6160(66)90207-0.

[19] ZHAO J H, DENG Y L, TANG J G, ZHANG J. Influence of strain rate on hot deformation behavior and recrystallization behavior under isothermal compression of Al-Zn-Mg-Cu alloy [J]. Journal of Alloys and Compounds, 2019, 809: 151788. DOI: 10.1016/j.jallcom.2019.151788.

[20] ZERILLI F J, ARMSTRONG R W. Dislocation-mechanics-based constitutive relations for material dynamics calculations [J]. Journal of Applied Physics, 1987, 61 (5): 1816−1825. DOI: 10.1063/1.338024.

[21] JAZAERI H, HUMPHREYS F J. The transition from discontinuous to continuous recrystallization in some aluminium alloys II − Annealing behaviour [J]. Acta Materialia, 2004, 52(11): 3251 − 3262. DOI: 10.1016/j.actamat.2004.03.031.

[22] HUMPHREYS F J. A unified theory of recovery, recrystallization and grain growth, based on the stability and growth of cellular microstructures—I. The basic model [J]. Acta Materialia, 1997, 45(10): 4231 − 4240. DOI: 10.1016/S1359-6454(97)00070-0.

[23] GHOLINIA A, HUMPHREYS F J, PRANGNELL P B. Production of ultra-fine grain microstructures in Al − Mg alloys by coventional rolling [J]. Acta Materialia, 2002, 50(18): 4461−4476. DOI: 10.1016/S1359-6454(02)00253-7.

[24] TAKAYAMA Y, SZPUNAR J A. Stored energy and taylor factor relation in an Al-Mg-Mn alloy sheet worked by continuous cyclic bending [J]. Materials Transactions, 2004, 45(7): 2316−2325. DOI: 10.2320/matertrans.45.2316

[25] SCHWARTZ A J, KUMAR M, ADAMS B L. Electron backscatter diffraction in materials science [M]. Springer, 2010.

[26] LIU Q, JUUL J D, HANSEN N. Effect of grain orientation on deformation structure in cold-rolled polycrystalline aluminium [J]. Acta Materialia, 1998, 46(16): 5819 − 5838. DOI: 10.1016/S1359-6454(98)00229-8.

[27] HU Y, LIU H, FUJII H. Improving the mechanical properties of 2219-T6 aluminum alloy joints by ultrasonic vibrations during friction stir welding [J]. Journal of Materials Processing Technology, 2019, 271: 75 − 84. DOI: 10.1016/j.jmatprotec.2019.03.013.

[28] KONIJNENBERG P J, ZAEFFERER S, RAABE D. Assessment of geometrically necessary dislocation levels derived by 3D EBSD [J]. Acta Materialia, 2015, 99: 402 − 414. DOI: 10.1016/j.actamat.2015.06.051.

[29] DOHERTY R D, HUGHES D A, HUMPHREYS F J, JONAS J J, JENSEN D J, KASSNER M E, KING W E, MCNELLEY T R, MCQUEEN H J, ROLLETT A D. Current issues in recrystallization: A review [J]. Materials Science and Engineering A, 1997, 238(2): 219 − 274. DOI: 10.1016/S0921-5093(97)00424-3.

(Edited by FANG Jing-hua)

中文导读

等温压缩及后续热处理对Al-Mg-Si合金晶粒结构演变的影响

摘要：研究了不同应变速率、温度和应变下变形的Al-Mg-Si合金本构关系。定量表征和分析了热变形和热处理过程中合金的等微观组织演变，包括再结晶分数、晶粒尺寸、局部位错取向、几何必要位错和储能之间的关系。结果表明，在热变形和后续热处理过程中，位错密度和储能与lnZ呈线性关系，说明两个过程中都发生了连续再结晶。随着lnZ的增加，位错密度在随后的热处理过程中下降更为明显。当lnZ小于28时，在热变形后的后续热处理过程中，位错密度随变形量的减小而趋于稳定。由于位错沿低角度晶界分布，亚晶在后续热处理过程中具有良好的稳定性。热变形过程中的主要再结晶机制是连续动态再结晶，并伴随高lnZ下的几何动态再结晶。

关键词：Al-Mg-Si合金；Zener-Hollomon参数；位错；再结晶；晶界